J Braz. Soc. Mech. Sci. Eng. (2015) 37:589–599
DOI 10.1007/s40430-014-0182-7

TECHNICAL PAPER

Vortex-induced vibration experiments with a long semi-immersed flexible cylinder under tension modulation: Fourier transform and Hilbert–Huang spectral analyses

Guilherme R. Franzini · Rodolfo T. Gonçalves · Celso P. Pesce · André L. C. Fujarra · Carlos E. N. Mazzilli · Julio R. Meneghini · Pedro Mendes

Received: 7 June 2013 / Accepted: 11 April 2014 / Published online: 21 June 2014

Abstract An experimental investigation of the vortex-induced vibration phenomenon on a long semi-immersed flexible cylinder in constant current profile were carried out at a recirculating water channel facility. The experiments are part of a comprehensive research project which aims a better understanding of non-linear riser dynamics. Vertical and prescribed monochromatic harmonic motions were imposed to the top with amplitude $A_t/L \approx 1\,\%$ causing eigenfrequencies modulations. The mass ratio parameter is $m^* \approx 10$, and the ratio between the total length L and the immersed length Lim is $L/Lim \approx 3.5$. The Reynolds number Re range lies within the interval $10^3 < Re < 10^4$. Three values of motion frequency f_t were imposed, being them $f_t : f_{N,1} = 1{:}3,\ 1{:}2$ and $1{:}1$ where $f_{N,1}$ is the first eigenfrequency. The application of both the Fourier Transform and the Hilbert–Huang Transform allowed identifying subharmonic components and also frequency modulation aspects in the data.

Keywords Vortex-induced vibrations · Flexible cylinder · Stiffness modulation and Hilbert–Huang transform.

1 Introduction

In the marine riser scenario, the structural dynamics is ruled by a complex combination of both linear and non-linear phenomena. A particular non-linear phenomenon of interest in the subject is the vortex-induced vibration (VIV).

VIV is one of the most studied fluid–structure interaction phenomenon and occurs if the frequency of vortex shedding fs (proportional to the free-stream velocity U_∞ and the structural diameter D) is close to one of the eigenfrequencies of the structure. The reviews by [2, 10, 20, 25] are surveys on the VIV theme.

As a non-linear resonant phenomenon, the VIV time scales are compared to those of the eigenperiods of the structure. There are also other characteristic time scales as those typical of offshore riser scenarios, excited by first- and second-order motions of the floating units. In a vertical riser arrangement, as an example, platform heave motions may cause tension oscillation at the top of the line, changing the geometric stiffness and modulating eigenfrequencies and, consequently, modulating VIV, see, e.g., [16, 21, 24].

Technical Editor: Celso Kazuyuki Morooka.

G. R. Franzini (✉) · C. P. Pesce (✉) · A. L. C. Fujarra
LMO-Offshore Mechanics Laboratory, Escola Politécnica, University of São Paulo, Av. Prof Mello Moraes, São Paulo 2231, Brazil
e-mail: gfranzini@usp.br

C. P. Pesce
e-mail: ceppesce@usp.br

G. R. Franzini · C. E. N. Mazzilli
LMC-Laboratory of Computational Mechanics, Escola Politécnica, University of São Paulo, São Paulo, Brazil

G. R. Franzini · R. T. Gonçalves · A. L. C. Fujarra
TPN-Numerical Offshore Tank, Escola Politécnica, University of São Paulo, São Paulo, Brazil

G. R. Franzini · J. R. Meneghini
NDF-Fluids and Dynamics Research Group, Escola Politécnica, University of São Paulo, São Paulo, Brazil

P. Mendes
Petrobras, Rio de Janeiro, Brazil

In this context, a comprehensive research project was carried out aiming at studying non-linear riser dynamics. One of the activities comprised fundamental experimental investigations of a long vertical and flexible cylinder subjected to tension modulated VIV phenomenon in constant current profile.

In a first round of experiments, in a recirculating water channel facility, the long cylinder was tested semi-immersed. In a second round of experiments, in a towing tank, the same long model was tested fully immersed. Those other experiments will be addressed in further works.

Experimental results with long and flexible cylinders subjected to VIV without top motion are presented in the papers by [3, 4] and by [14, 15]. In Huera-Huarte's work, as in the present paper, only the lower part of the model is immersed in water. On the other hand, Chaplin's experiments employed a vacuum chamber so that the lower part of the model is immersed in a constant current. This avoids discontinuities on tension and on hydrodynamics coefficients along the cylinder span.

Experimental investigations regarding the effects of the stiffness modulation on the VIV phenomenon are, however, rarer. The papers by [5, 6] studied an analogous modulated VIV phenomenon. In that case, a rigid cylinder was fixed to a controlled leaf spring in which the elastic stiffness may be modulated. The authors pointed out that the rate of frequency modulation affects the oscillation amplitude plot.

Due to the non-linear and non-stationary character of the VIV, standard signal analysis techniques based on Fourier Transform may not be sufficient to deal with the richness of aspects observed in the experiments. In this scenario, the Hilbert–Huang Transform (HHT) technique, introduced by [13], appears as a useful method to take into account amplitude and frequency modulations and multimodal behavior embedded in the signals.

The HHT has been employed on VIV investigations concerning a rigid cylinder assembled to elastic supports, cantilevered cylinders and elastically mounted flexible cylinder, as can be found in a series of papers recently published (see [5–8, 11, 17]).

The focus of the present paper is to carry out an analysis of such non-linear and frequency modulated phenomenon using both the Fourier-based method (power spectrum density—PSD) and the time–frequency domain, Hilbert–Huang Transform, showing how this latter technique can offer a complementary understanding of the experimental results.

2 Experimental arrangement and analysis methodology

Experiments were carried out at the recirculating water channel facility at the Fluids and Dynamics Research Group (NDF) at Escola Politécnica. The recirculating water channel test section has dimensions $700 \times 700 \times 7,500$ mm and can operate at low level of turbulence ($\approx$2 %) in free-stream velocities up to $U_\infty = 0.4$ m/s. A more detailed discussion regarding this facility can be found in [1].

The flexible cylinder is $L_t \approx 2500$ mm long, has diameter of $D = 22.2$ mm and immersed length $L \approx 720$ mm. The Reynolds number $Re = U_\infty D/\nu$ (ν is the kinematic viscosity of the fluid) ranges in the interval $10^3 < Re < 10^4$. The tested model is made of a flexible silicon tube completely filled with stainless steel microspheres, leading to a mass ratio parameter[1] $m^* = ms/md \approx 10$. Free-oscillation tests in still water allowed identifying the structural damping ratio corresponding to the first eigenmode as $\zeta_s^1 \approx 1$ % (see Fig. 1). The eigenfrequencies followed a linear relationship with the mode, i.e, $f_{N,i} = if_{N,1}, \quad i = 2, 3, 4$. See [21] for detailed discussions on this subject. The small-scale model was designed aiming at reaching a certain degree of possible dynamic similarity with a full-scale riser; see [19]. In fact, top motion, caused by the floating unity in full scale, induces adopting Froude's number identity as a primary scaling law. Accordingly, added mass coefficients and weight similarities take care of natural period similarity. Moreover, structural parameters, as bending and axial stiffness, were preserved in small scale. A discussion on Reynolds number and Keulegan–Carpenter number can be also found in [19]. The same model was also tested fully immersed in a towing tank facility. This latter set of experiments will be explored in future works.

In typical offshore scenarios, the Reynolds number and mass ratio parameter orders are 10^5 and 10 , respectively. Notice that the full-scale Reynolds numbers are much larger than those in the investigation herein described. This aspect is in fact a limitation of the laboratory experiments. The importance of Re effects on VIV has been focus of many investigations on the theme (see [12] and [18]).

On the other hand, m^* is one order above the characteristic value for offshore applications (typically $m^* \approx 2$). As mentioned, the model is precisely the same one employed in fully immersed experiments. In that case, m^* is close to typical values found in the offshore engineering. Further investigations will include the comparison between these two cases, discussing the effects of m^* and the discontinuities in the hydrodynamic damping and added mass observed in the semi-immersed one.

Monochromatic vertical motion was imposed to the upper extremity of the flexible cylinder at distinct frequencies f_t using a specific and in-house built servomotor device. A major experimental issue is to measure the

[1] Ratio between the structural oscillating mass and the mass of fluid displaced by the body.

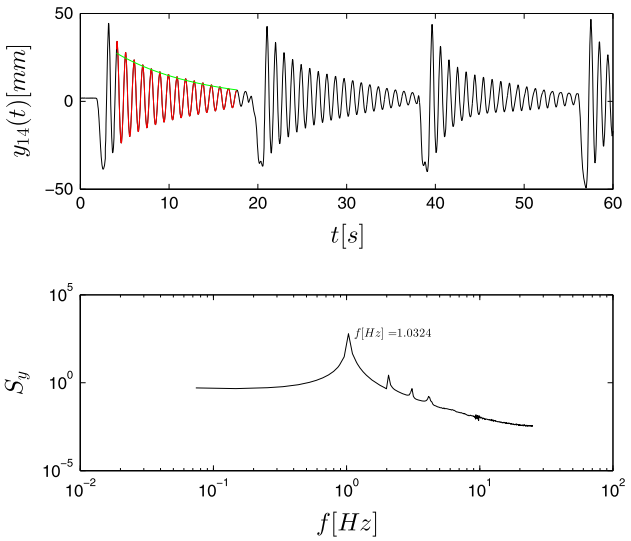

Fig. 1 Free-oscillation tests result in still water

elastica as a function of time. For this, cartesian coordinates of 43 reflexive targets placed along the model were acquired through an optical tracking system. A load cell measured the tension at the top. Figure 2 presents both the sketch and a picture of the experimental setup.

Four cameras acquired the data from the non-immersed targets, while two submerged cameras acquired the signals from the immersed ones. The submerged cameras were installed more than 1 m downstream the flexible cylinder aiming at avoiding interference effects. The calibration procedure consisted in acquiring the random motion of a calibration frame composed by two reflexive targets. The uncertainty of the measurement is typically 0.1 mm. The time series obtained from the submerged and aerial cameras were synchronized and referred to the same axes, as defined in Fig. 2a.

Each run lasted 180 s. The setup time for a new stationary current regime was taken as 120 s. All the signals were acquired with sample frequency $fsp = 50$ Hz. For each target, the oscillation amplitude was evaluated taking the averaged value of the 10 % of the larger peaks, similarly to what was carried out in [9].

Regarding the spectral analysis methodology, two different approaches are employed. The first one consists in making use of the usual Fourier Transform to obtain the PSD. The whole PSD analysis was carried out cutting off the DC component. The second approach is based on the use of the Hilbert–Huang Transform. For both approaches, the frequency is normalized by the first eigenfrequency of the installed flexible cylinder $f_{N,1} \approx 1$ Hz.

3 Experimental results and discussion

The cartesian coordinates (normalized by the diameter D) in the in-line, transversal and axial directions ($x^*(t)$, $y^*(t)$ and $z^*(t)$, respectively) will be analyzed, just focusing the target numbered 13. This point is not a node for either the first or the second eigenmodes. The vertical position (at rest) of this target is close to 45 mm (2 diameters) above the air–water interface. This paper will focus only on the analysis of two reduced velocities $V_{R,1} = U_\infty / f_{N,1} D = 4.99$ and $V_{R,1} = 10.34$. These correspond to the VIV amplitude peaks related to the first and second eigenfrequencies.

This section is divided into three subsections. In the first one, the oscillation amplitude, A_y^*, is plotted as function of the spanwise position for the mentioned reduced velocities. This result is a straightforward way for numerical experimental comparisons.

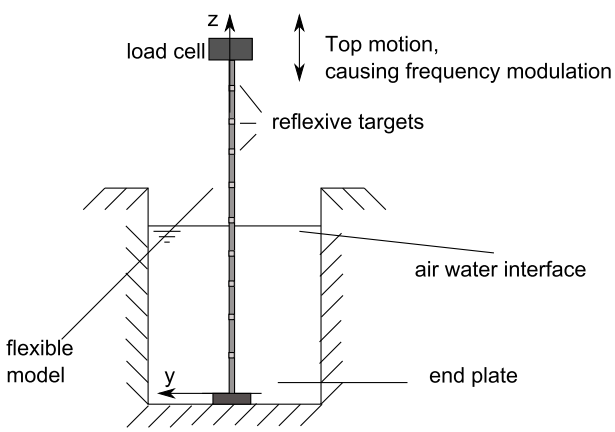

(a) Front view sketch.

(b) Picture.

Fig. 2 Experimental setup. Note the reflexive markers along the cylinder. Free-stream velocity is in ***i*** direction

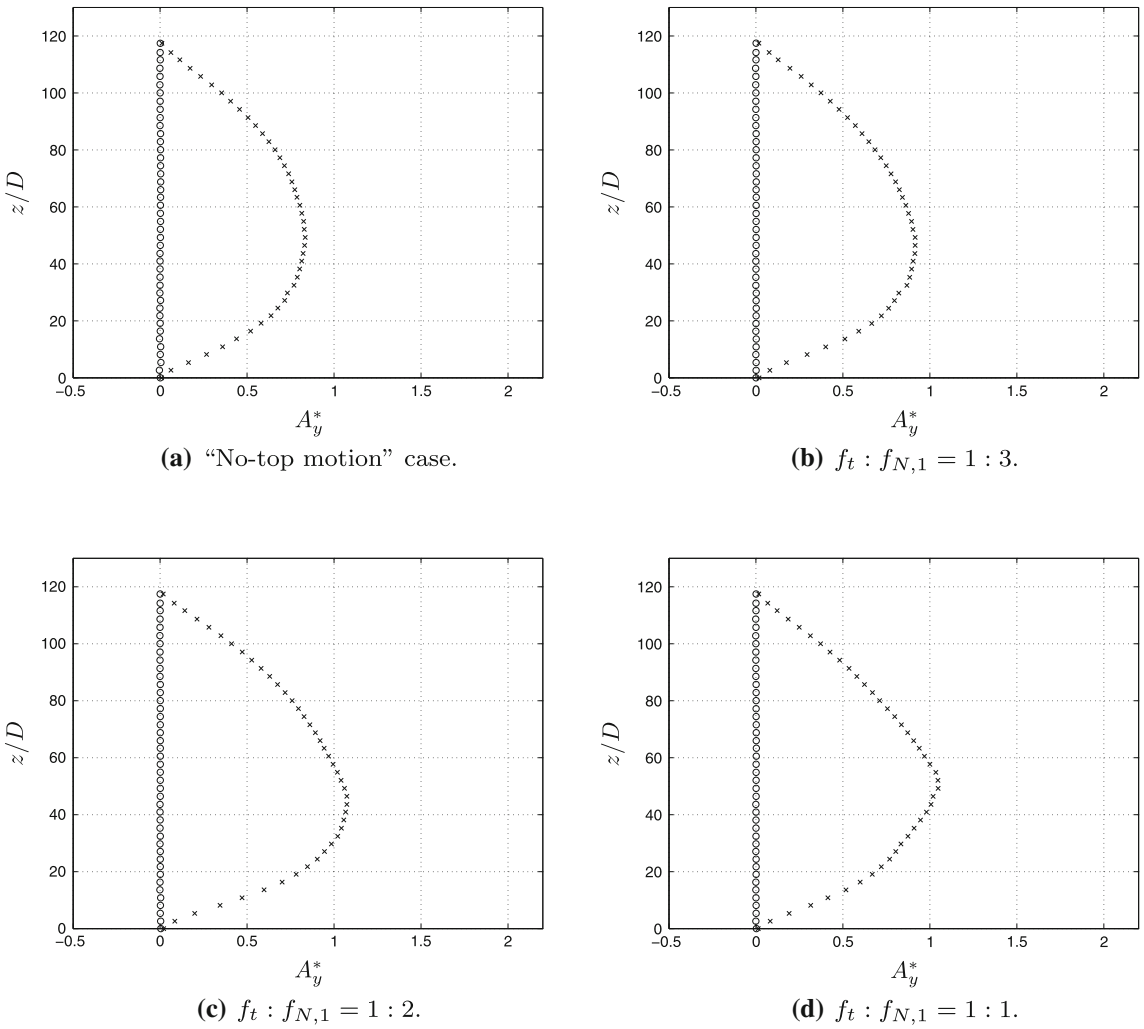

(a) "No-top motion" case. **(b)** $f_t : f_{N,1} = 1 : 3$.

(c) $f_t : f_{N,1} = 1 : 2$. **(d)** $f_t : f_{N,1} = 1 : 1$.

Fig. 3 Oscillation amplitude $A_y(z^*)$: $V_{R,1} = 4.99$

The next two subsections focus on the comparison between Fourier and Hilbert–Huang Spectra computed from $y^*(t)$ for the considered target.

3.1 Oscillation amplitude

Figure 3 presents the oscillation amplitude in transverse direction A_y^* as function of the spanwise position z^* for the $V_{R,1} = 4.99$ case. As expected from analogy with the case in which a rigid cylinder is mounted on elastic support, the lock-in occurs in the first eigenmode. Notice that the presence of prescribed top motion increases the maximum oscillation amplitude from 0.7 diameters (only current, "no-top motion" case) to a value slightly larger than 1 diameter, as in the case $f_t : f_{N,1} = 1 : 1$.

The same plot for $V_{R,1} = 10.4$ indicates interesting results. At this reduced velocity, lock-in with the second eigenmode is expected, fact confirmed in the "no-top motion" case (see Fig. 4a).

For the conditions $f : f_{N,1} =$ 1:3 and 1:2 (Fig. 4b, c, respectively), it is clearly the concomitance of the first and second eigenmodes. Notice that the contribution of the first eigenmode increases with the top motion frequency. In the case $f_t : f_{N,1} =$ 1:1, shown in Fig. 4d, the contribution of the first eigenmode is dominant if compared to that of the second eigenmode.

3.2 Spectral analysis for $V_{R,1} = 4.99$

Displacement time series and corresponding spectral analysis are presented in Fig. 5. The "no-top motion" condition results present narrow band spectral distribution, as can be seen in Fig. 5a. For this case, the frequency with the higher amount of energy, the dominant one, is close to the first eigenfrequency, which indicates that the VIV is synchronized with this eigenfrequency for both in-line and cross-flow directions. Notice also the presence of a $f : f_{N,1} = 2$ subharmonic component in the in-line spectrum.

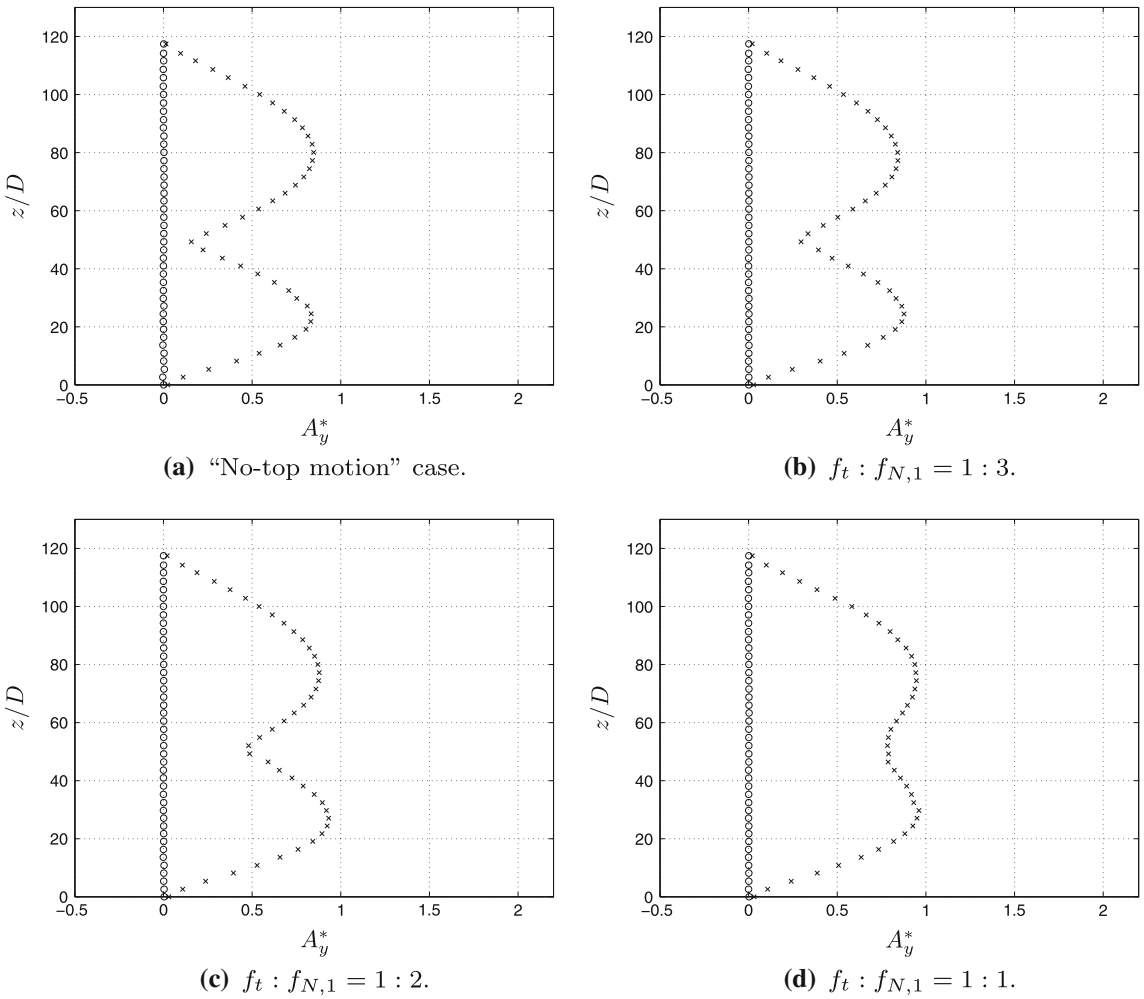

Fig. 4 Oscillation amplitude $A_y(z^*)$: $V_{R,1} = 10.4$

For the same reduced velocity, but in the top motion cases, with $f_t : f_{N,1} =$ 1:3 and $f_t : f_{N,1} =$ 1:2 (Fig. 5b, c, respectively) a richer presence of subharmonic components is visible. For the $f_t : f_{N,1} =$ 1:3 case, the in-line spectrum presents the components $f : f_{N,1} =$ 1:3; 2:3; 3:3; 4:3; 5:3 and 6:3. Similarly, the in-line spectrum for the $f_t : f_{N,1} =$ 1:3 case is composed by the components $f : f_{N,1} =$ 1:2; 2:2; 3:2 and 4:2.

This spectral distribution can be explained with simple arguments. It is worth to emphasize that non-linear modes and reduced order models approaches could also be applied, similarly to [22] and [23]. Let q being the generalized modal coordinate, m_q, c_q and $k_q(t)$ the modal quantities related to mass, damping and stiffness of the system. Notice that, in the top motion cases, the modal stiffness is a function of time. The motion equation can be approximately written, within a first simple linear modeling, as:

$$m_q\ddot{q} + c_q\dot{q} + k_q(t)q = F_q(t) \tag{1}$$

If we consider that the response is harmonic and monochromatic, that is, $q(t) = Q\cos(\Omega_{N,1}t)$ and that the modal stiffness is given by

$$k_q(t) = \overline{k_q} + \Delta k_q \cos(\Omega_t t) \tag{2}$$

The equation of motion is written:

$$m_q\ddot{q} + c_q\dot{q} + \overline{k_q}q = F_q(t) - \Delta k_q Q\cos(\Omega_{N,1}t)\cos(\Omega_t t) \tag{3}$$

Through basic trigonometric relationships, we can rewrite Eq. 3 as:

$$m_q\ddot{q} + c_q\dot{q} + \overline{k_q}q = F_q(t) - \frac{\Delta k_q Q}{2}\left[\cos\left(\left[\Omega_{N,1} + \Omega_t\right]t\right) + \cos\left(\left[\Omega_{N,1} - \Omega_t\right]t\right)\right] \tag{4}$$

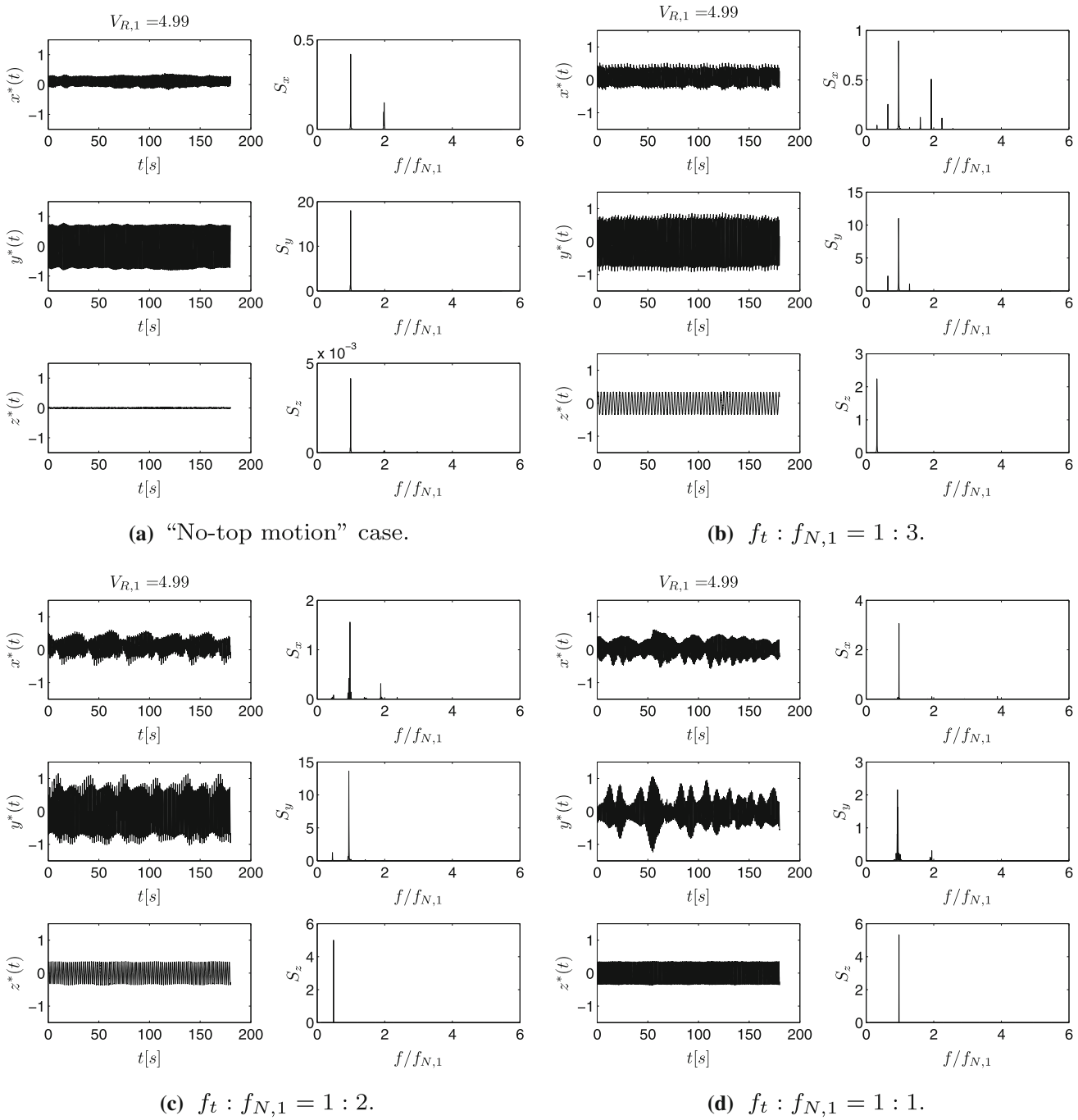

(a) "No-top motion" case.

(b) $f_t : f_{N,1} = 1 : 3$.

(c) $f_t : f_{N,1} = 1 : 2$.

(d) $f_t : f_{N,1} = 1 : 1$.

Fig. 5 Time series of displacements and PSDs: Response to a top motion amplitude $A_t = 1\,\%Lt$, at $V_{R,1} = 4.99$. Target number 13

The right-hand side member of Eq. 4 clearly shows that there is a forcing term due to the stiffness modulation composed by two frequencies, namely the sum frequency $\Omega_{N,1} + \Omega_t$ and a difference frequency $\Omega_{N,1} - \Omega_t$.

As mentioned, the in-line response spectrum presents the components $f : f_{N,1} =$ 1:3; 2:3; 3:3; 4:3, which, respectively, correspond to the "top motion" frequency, the "difference frequency", the first eigenfrequency and the "sum frequency". Thus, the response is similar to that which would be obtained with a linear system forced by these distinct frequencies. Similar analysis can be carried out for the case with $f_t := f_{N,1} =$ 1:2.

The experimental results for $f_t : f_{N,1} =$ 1:1, shown in Fig. 5d, present a narrow band spectra centered in $f_{N,1} = f_t$. Clearly, the cross-flow displacement time series is non-stationary. In this scenario, the Hilbert–Huang Transform

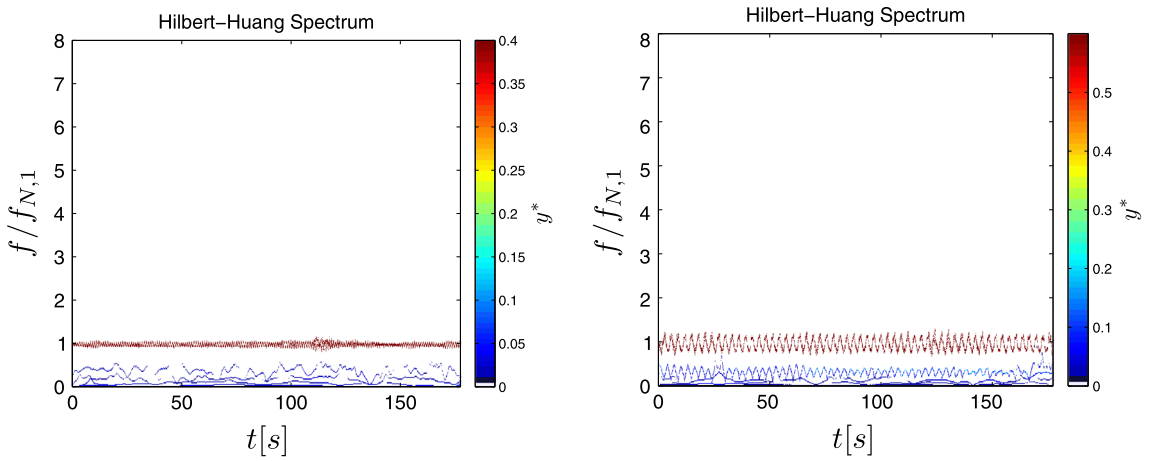

(a) "No-top motion" case. **(b)** $f_t : f_{N,1} = 1 : 3$.

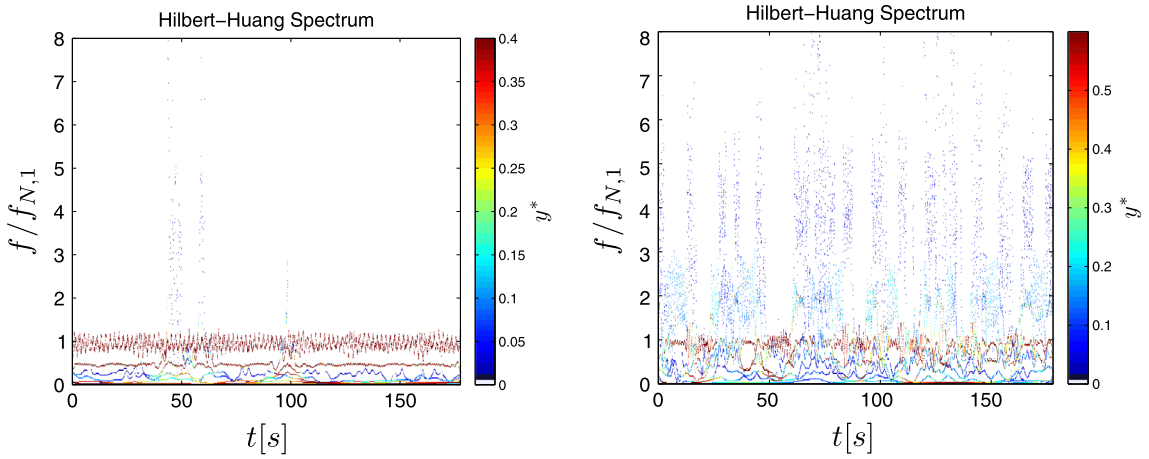

(c) $f_t : f_{N,1} = 1 : 2$. **(d)** $f_t : f_{N,1} = 1 : 1$.

Fig. 6 Cross-flow amplitude Hilbert–Huang Spectrum: $V_{R,1} = 4.99$; target number 13

may offer another perspective for the interpretation of results.

Figure 6 presents the Hilbert–Huang spectra for the cross-flow oscillations time series at reduced velocity $V_{R,1} = 4.99$. The "no-top motion case" (Fig. 6a) shows that the highest amount of energy is contained in the oscillations with $f/f_{N,1} \approx 1$. Notice that the response frequency modulation is negligible during the time spanned by the experiments.

The "top motion" cases with $f_t : f_{N,1} = 1 : 3$ and 1:2 (Fig. 6b, c, respectively) are characterized by frequency modulation around $f \approx f_{N,1}$ and also by another frequency trace close to the top motion frequency. It is worth mentioning that this last frequency trace has lower energy level. Curiously, traces corresponding to sum and difference frequencies are not strictly observed in the Hilbert–Huang spectra. In fact, in HHT analysis, these distinct frequencies are replaced by a continuous and modulated frequency trace, whose frequency of modulation matches the frequency of the imposed top motion. This is certainly an issue deserving further and deeper considerations.

The Hilbert–Huang spectrum for the $f_t : f_{N,1} = 1{:}1$ case is shown in Fig. 6d. In contrast to the previous cases, this frequency trace around $f \approx f_{N,1}$ presents a marked non-regular amplitude modulation. In addition, both the amplitude and frequency traces of the other components of the Hilbert–Huang spectrum present a more complex distribution, if compared to the other exciting frequencies cases.

3.3 Spectral analysis for $V_{R,1} = 10.34$

The analysis will focus now on the results for reduced velocity $V_{R,1} = 10.34$. Figure 7 presents the cartesian displacements for the same target and the corresponding PSD plots. As expected, the mean value of the in-line oscillations

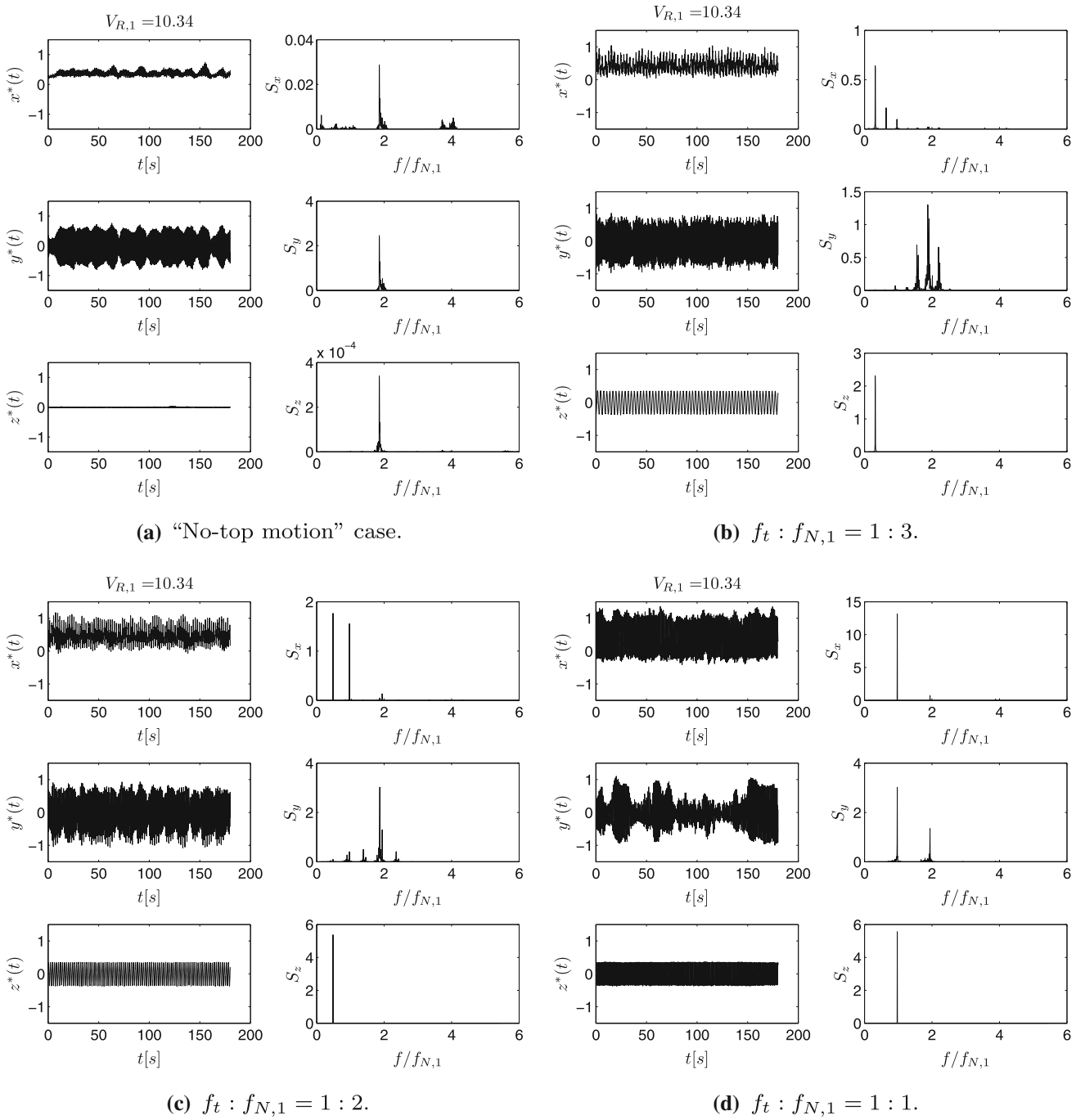

(a) "No-top motion" case.

(b) $f_t : f_{N,1} = 1 : 3$.

(c) $f_t : f_{N,1} = 1 : 2$.

(d) $f_t : f_{N,1} = 1 : 1$.

Fig. 7 Time series of displacement and PSD: Response to a top motion amplitude $A_t = 1\,\%L_t$, at $V_{R,1} = 10.34$; target number 13

are higher than those observed in the experiments at $V_{R,1} = 4.99$ caused by the higher value of the mean hydrodynamic drag force.

The cross-flow displacement times-series for the "no-top motion" case are presented in Fig. 7a. The narrow band spectrum indicates the synchronization with the second eigenfrequency. Regarding the in-line spectrum, the synchronization is also observed with the second eigenmode, despite the presence of energy contained in the $f : f_{N,1} = 4{:}1$ subharmonic.

The $f_t : f_{N,1} =$ 1:3 and 1:2 experiments (Fig. 7b, c, respectively) present similar results. The narrowband in-line displacement spectra are composed by the sum and difference frequencies in relation to the first eigenfrequency. The cross-flow spectra also present narrowband characteristics. The sum and difference frequencies are also

observable in these spectra, but now they are centered around the second eigenfrequency.

The time series and the corresponding spectra for the $f_t : f_{N,1} =$ 1:1 case are shown in Fig. 7d. The in-line spectrum is practically monochromatic with the same frequency of the top motion, whereas the cross-flow spectrum is composed mainly by two frequencies, namely the first and second eigenfrequencies. Similarly to the analysis at reduced velocity $V_{R,1} = 4.99$, non-stationary and modulated character of $y^*(t)$ is clearly visible and may not have been taken into account precisely. Again, the use of the Hilbert–Huang Transform may offer a complementary view to the Fourier Transform-based method.

Figure 8 presents the Hilbert–Huang Spectra corresponding to the cross-flow amplitude time series. The "no-top motion" case spectrum (Fig. 8a) is very similar to that obtained at $V_{R,1} = 4.99$, with almost no frequency or amplitude modulations. The difference is only perceivable in the typical frequency of oscillation, here centered around $f \approx 2f_{N,1}$, in contrast to the previous case.

The results for the $f_t : f_{N,1} =$ 1:3 and 1:2 experiments are shown in the Fig. 8b, c. Similarities were also found in the $V_{R,1} = 4.99$ cases. The sum and difference frequencies are replaced by a continuous frequency trace, now centered in $f \approx 2f_{N,1}$, and the frequency of modulation matches that from the top motion. It is also observable the presence of the components $f \approx f_{N,1}$ and $f \approx f_t$ in both the Hilbert–Huang spectra. One can notice that these two last frequencies components present lower energy level and also lower frequency modulation than the $f \approx 2f_{N,1}$ component, despite the stiffness modulations.

Another interesting aspect that was also observed in the results of the lower reduced velocity is related to the width of the frequency oscillation band. For both the reduced velocities, this width seems to be invariant with respect to the top motion frequency, depending only on the reduced velocity. The larger the reduced velocity, the larger is the width. This aspect is not given by the PSD plot and deserves further investigations.

Finally, the Hilbert–Huang Spectrum for the $f_t : f_{N,1} =$ 1:1 case is presented in Fig. 8d. Two most energetic components are sparsely observed around $f \approx 2f_{N,1}$ and $f \approx f_{N,1}$. It is worth mentioning that this latter frequency is the top motion one, which matches the first eigenfrequency.

Similarly to what has been observed in the $f_t : f_{N,1} =$ 1:3 and 1:2 cases, the frequency component around $f \approx 2f_{N,1}$ is characterized to be more pronouncedly modulated than the $f \approx f_{N,1}$ one. Notice also that, within the interval in which the larger amplitudes are observed in the $f \approx 2f_{N,1}$ component, larger amplitudes are reported for the $f \approx f_{N,1}$ component. We speculate that there are at least two synchronization regimes. One between the vortex shedding and the displacement, which consists on the classical VIV synchronization; and another between the top motion and the displacement. This aspect is also under investigation and certainly deserves a more detailed analysis to be published in a future work.

4 Summary and concluding remarks

Experiments of vortex-induced vibrations with a semi-immersed long flexible cylinder subjected to constant current profiles were carried out at a recirculating water channel facility. The cartesian displacements of 43 targets placed along the model were acquired using an optical tracking system. Vertical and monochromatic top motions were imposed to the structure, causing geometric stiffness modulation. Besides the "no-top motion" case, three levels of frequency were imposed $f_t : f_{N,1} =$ 1:3; 1:2 and 1:1.

The focus of the paper was to analyze the displacement time series of one target at two reduced velocities conditions (namely $V_{R,1} = 4.99$ and 10.34) corresponding to the first two VIV amplitude peaks using both Fourier based analysis and the Hilbert–Huang Transform. The main objective is to carry out a comparative analysis with these distinct techniques, showing the revealed aspects.

Considering the reduced velocity $V_{R,1} = 4.99$, the PSD plots obtained from the "no-top motion" case show narrow band characteristics for the in-line and cross-flow spectra, with dominant frequency corresponding to the first eigenfrequency. The spectral analysis of the cases $f_t : f_{N,1} =$ 1:3 and 1:2 presented clearly sum and difference components. This spectral distribution can be explained with a simple linear dynamic argument. The cross-flow oscillation for the $f_t : f_{N,1} =$ 1:1 case is characterized by amplitude modulations. In this context, the PSD plot may not take into account all the characteristics embedded in the data.

No significant frequency modulation was observed in the Hilbert–Huang Spectrum corresponding to the "no-top motion" cases. In the cases with $f_t : f_{N,1} =$ 1:3 and 1:2, the sum and difference frequencies were replaced by a continuous frequency time trace. The period of frequency modulation matched the period of the prescribed top motion. As expected from the analysis of the time series, the Hilbert–Huang Spectrum for the $f_t : f_{N,1}$ was able to capture the amplitude modulations.

For the experiments with $V_{R,1} = 10.34$, the "no-top motion" case presented similar spectral distribution, but centered at the second eigenfrequency. In the cases in which the top motion conditions were $f_t : f_{N,1} =$ 1:3 and 1:2, a richer spectral distribution was observed. Similarly to the previous reduced velocity analysis, the sum and

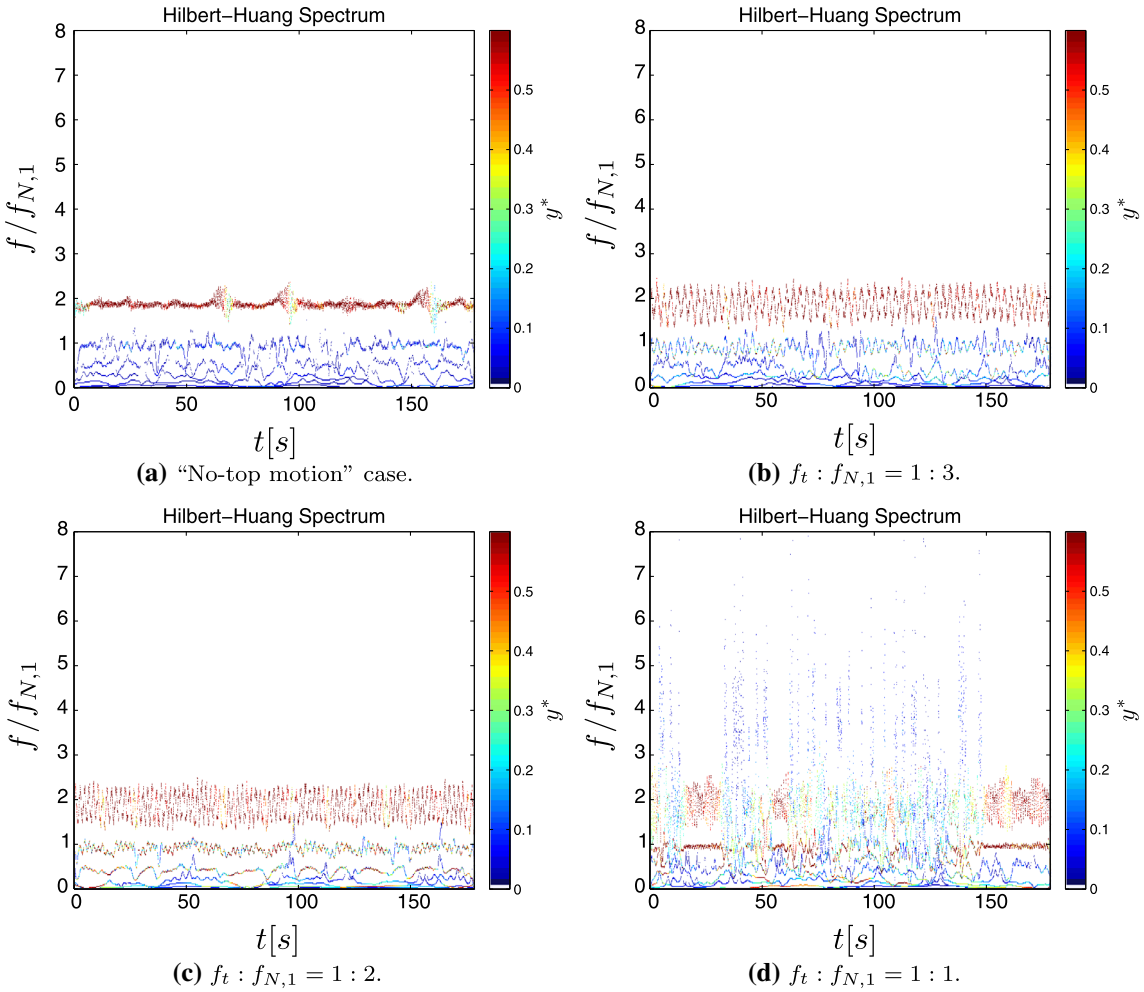

(a) "No-top motion" case. **(b)** $f_t : f_{N,1} = 1 : 3$. **(c)** $f_t : f_{N,1} = 1 : 2$. **(d)** $f_t : f_{N,1} = 1 : 1$.

Fig. 8 Cross-flow Hilbert–Huang Spectrum: $V_{R,1} = 10.34$

difference frequency components were presented at the PSD plot. Significant amplitude modulation was observed in the $f_t : f_{N,1} = 1{:}1$ case.

The Hilbert–Huang Spectrum for the "no-top motion" case did not show significant frequency modulation, in agreement with the results obtained at $V_{R,1} = 4.99$. Another similarity observed with the lower reduced velocity concerned the fact that, for the conditions $f_t : f_{N,1} = 1{:}3$ and $1{:}2$, the most energetic component showed up around the dominant frequency obtained from the PSD analysis and this component presented a period of oscillation that matches the period of the imposed top motion. The bandwidth in which the frequency of oscillation varied is larger than the one observed for $V_{R,1} = 4.99$ but seems to be independent of the top motion frequency.

The results showed that the complimentary use of the PSD plots and the Hilbert–Huang spectrum is a fruitful analysis tool for the data obtained from a non-linear system under parametric excitation. The PSD plots indicate the existence of sum and difference frequencies, besides the fundamental one. On the other hand, in the HHT analysis, these three oscillation frequencies are replaced by a continuous frequency time trace. It is worth to be highlighted that the bandwidth of this trace of frequency depends on the value of the reduced velocity, but seems to be independent of the top motion frequency. The interpretation given by the HHT is physically sounder, since clearly shows the oscillation frequency modulating with the natural frequency. The complementary information given by both techniques allowed identifying some dynamic characteristics, mainly related to the different time scales. In the particular case of offshore applications, a better understanding of this dynamics can be used in fatigue analysis methodologies.

Further analysis may comprise the full set of data, taken all along the flexible cylinder aiming at a more comprehensive picture of the dynamics. Modal decomposition techniques together with Fourier and HHT would enhance the analysis.

Finally, experimental analyses with the whole model immersed are presently being carried out. The fully immersed condition leads to a mass ratio parameter close to the one observed in real risers and offshore structures, among others aspects.

Acknowledgments The authors would like to acknowledge FAPESP, FINEP, Petrobras and CNPq for sponsoring VIV researches at the University of São Paulo. First author is grateful to FAPESP for his post-doctoral scholarship (process 2013/09802-2). Fourth author is grateful to the Brazilian Navy for all support provided during his sabbatical period, 2011–2012. Mr. Douglas Silva is also acknowledged for his help with the experimental apparatus.

References

1. Assi GRS, Meneghini JR, Aranha JAP, Coleto WGP (2005) Design, assembling and verification of a circulating water channel facility for fluid dynamics experiments. In: Proceedings of COBEM05—18th international congress of mechanical engineering
2. Bearman PW (1984) Vortex shedding from oscillating bluff bodies. Annu Rev Fluids Mech 16:195–222
3. Chaplin JR, Bearman PW, Cheng Y, Fontaine E, Graham JMR, Herfjord K, Huera Huarte FJ, Isherwood M, Lambracos K, Larsen CM, Meneghini JR, Moe G, Pattenden R, Triantafyllou MS, Willden RHJ (2005) Blind predictions of laboratory measurements of vortex-induced vibrations of a tension riser. J Fluids Struct 21(1):25–40
4. Chaplin JR, Bearman PW, Huera Huarte FJ, Pattenden RJ (2005) Laboratory measurements of vortex-induced vibrations of a vertical tension riser in a stepped current. J Fluids Struct 21:3–24
5. Franzini GR, Pereira AAP, Fujarra ALC, Pesce CP (2008) Experiments on VIV under frequency modulation and at constant Reynolds number. In: Proceedings of OMAE 08, 27th international conference on offshore mechanics and arctic engineering
6. Franzini GR, Pesce CP, Gonçalves RT, Fujarra ALC, Meneghini JR (2010) An experimental investigation on frequency modulated VIV in a water channel. In: IUTAM symposium on bluff bodies wakes and vortex-induced vibrations—BBVIV6
7. Franzini GR, Pesce CP, Gonçalves RT, Fujarra ALC, Pereira APP (2011) Concomitant vortex-induced vibration experiments: a cantilevered flexible cylinder and a rigid cylinder mounted on a leaf-spring apparatus. In: Proceeding of the XIV international symposium on dynamic problems of mechanics DINAME 2011
8. Franzini GR, Pesce CP, Gonçalves RT, Fujarra ALC, Pereira APP (2011) Analysis of multimodal vortex-induced vibrations using the Hilbert–Huang spectral analysis. In: Proceeding of the third international conference on Hilbert–Huang transform: theory and applications
9. Franzini GR, Gonçalves RT, Meneghini JR, Fujarra ALC (2013) One and two degrees-of-freedom vortex-induced vibration experiments with yawed cylinders. J Fluids Struct 42:401–420
10. Gabbai R, Benaroya H (2005) An overview of modeling and experiments of vortex-induced vibration of circular cylinders. J Fluids Struct 282:575–616
11. Gonçalves RT, Franzini GR, Rosetti GF, Fujarra ALC, Nishimoto K (2012) Analysis methodology for vortex-induced motion (VIM) of a monocolumn platform applying the HilbertHuang transform method. J Offshore Mech Arct Eng 134:011103-1–011103-7
12. Govardhan RN, Williamson CHK (2006) Defining the "modified Griffin plot" in vortex-induced vibration: revealing the effect of Reynolds number using controlled damping. J Fluid Mech 561:147–180
13. Huang NE, Shen Z, Long SR, Wu MC, Shih HH, Zheng Q, Yen N, Tung CC, Liu HH (1998) The empirical mode decomposition and the Hilbert spectrum for nonlinear and non-stationary time series analysis. R Soc Lond 454:903–955
14. Huera-Huarte FJ, Bearman PW (2009) Wake structures and vortex-induced vibrations of a long flexible cylinder—part 1: dynamic response. J Fluids Struct 25:969–990
15. Huera-Huarte FJ, Bearman PW (2009) Wake structures and vortex-induced vibrations of a long flexible cylinder—part 2: drag coefficients and vortex modes. J Fluids Struct 25:991–1006
16. Josefsson PM, Dalton C (2010) An analytical/computational approach in assessing vortex-induced vibration of variable tension riser. J Offshore Mech Arct Eng 132:031302-1–031302-7
17. Pesce CP, Fujarra ALC, Kubota L (2006) The Hilbert–Huang spectral analysis method applied to VIV. In: Proceedings of the 25th international conference on offshore mechanics and artic engineering OMAE2006, Hamburg, Germany
18. Raghavan K, Bernitsas MM (2010) Experimental investigation of Reynolds number effect on vortex induced vibration of rigid circular cylinder on elastic supports. Ocean Eng 38:719–731
19. Rateiro F, Pesce CP, Gonalves RT, Franzini GR, Fujarra ALC, Salles R, Mendes P (2012) Risers model tests: scaling methodology and dynamic similarity. In: Proceedings of the the 22nd international ocean and polar engineering conference, ISOPE 2012
20. Sarpkaya T (2004) A critical review of the intrinsic nature of vortex-induced vibrations. J Fluids Struct 19:389–447
21. Silveira LMY, Martins CA, Cunha LD, Pesce CP (2007) An investigation on the effect of tension variation on VIV of risers. In: Proceedings of the 26th international conference on offshore mechanics and artic engineering OMAE2007, San Diego, USA
22. Srinil N, Wiercigroch M, O'Brien P (2009) Reduced-order modelling of vortex-induced vibration of catenary riser. Ocean Eng 36:1404–1414
23. Srinil N (2010) Multi-mode interactions in vortex-induced vibrations of flexible curved/straight structures with geometric nonlinearities. J Fluids Struct 26:1098–1122
24. Srinil N (2011) Analysis and prediction of vortex-induced vibrations of variable-tension vertical risers in linearly sheared currents. Appl Ocean Res 33:41–53
25. Williamson CHK, Govardhan RN (2004) Vortex-induced vibrations annual. Rev Fluids Mech 36:413–455